RSC Advances

COMMUNICATION

View Article Online
View Journal | View Issue

Cite this: *RSC Adv.*, 2016, **6**, 3742

Received 10th October 2015
Accepted 14th December 2015

DOI: 10.1039/c5ra21020h

www.rsc.org/advances

Binder-free integration of insoluble cubic CuCl nanoparticles with a homologous Cu substrate for lithium ion batteries

Song Liu,[a] Hongying Hou,*[a] Wen Hu,[a] Xianxi Liu,[b] Jixiang Duan[a] and Ruijin Meng[a]

Binder-free integration of a novel insoluble cubic cuprous chloride (CuCl) nanoparticle anode material with homologous Cu foil was designed and achieved *via* facile *in situ* electrochemical self-assembly for the first time. The integrated CuCl/Cu electrode for lithium ion batteries was studied in terms of SEM, EDX, XRD, galvanostatic charge/discharge, cycle stability, rate performance, cyclic voltammograms (CV) and AC impedance. As expected, insoluble cubic CuCl nanoparticles did *in situ* grow and tightly combine with the surface of Cu foil, and the resultant CuCl/Cu electrode delivered a reversible discharge capacity of 250.6 mA h g^{-1} after 300 cycles at 2C, indicating satisfactory cyclic stability. In addition, the corresponding Li^+ diffusion coefficient was calculated to be 1.8×10^{-11} cm^2 s^{-1}, higher than that of the MnO anode material in literature. Binder-free integration of homologous materials *via* self-assembly can not only ensure the tight combination of insoluble CuCl nanoparticles with Cu foil, but also avoid negative effects due to the polymer binder on electrochemical performance.

1 Introduction

Although graphite is intensively used as the anode active material in commercial lithium ion batteries (LIBs), the easy formation of Li-dendrites and SEI films also discount the safety and the electrochemical performance.[1,2] Therefore, many alternative anode active materials (such as Sn, Al, Ge, MnO, CuO, and ZnO) are constantly being proposed and investigated.[3–6] Each of these materials possesses its own merits and more, or less, Li-storage capacity. However, opportunities coexist with challenges, and their advantages can also be offset. For example, metal-based anode active materials deliver high discharge capacities; however, they also suffer from poor cyclability due to large volume changes and pulverization during long term cyclic lithiation/de-lithiation.[6–8] In the case of transition metal oxides, the inherent poor electrical conductivity results in inferior cyclability.[9,10] Therefore, it is interesting and desirable to continuously explore novel anode active materials with better electrochemical performances.

Unlike transition metal oxides, most transition metal chlorides are soluble in aqueous solutions; consequently, the corresponding electrochemical conversion reactions with Li^+ are easily neglected and rarely reported. Recently, attention has been paid to several metal chlorides (such as $CuCl_2$ and AgCl) for the anode active materials in LIBs, but not insoluble CuCl.[11,12] In addition, most of the manufacturing technologies for the electrode often involve the use of insulating polymer binders, and the inertness of the insulating polymer binder to Li-storage activity may block the transport pathway of Li^+ and electrons to some degree, which may slow down the kinetic process of the electrode and decrease the specific discharge capacity. Therefore, binder-free integration of active materials with the current collector *via* self-assembly can not only avoid the negative effects of the polymer binder, but also simplify the fabrication process of the electrode, which would be preferable for three-dimensional micro LIBs.[13,14] In principle, compared with soluble metal chlorides, very low solubility in the aqueous electrolyte can facilitate *in situ* deposition of solid CuCl and binder-free integration with Cu substrate *via* a facile one-step anodization procedure. However, the corresponding reports about CuCl anode active materials in LIBs are still scarce.

In this study, such an effort was made for the first time: tight binder-free integration of insoluble cubic CuCl nanoparticles with homologous Cu current collector for a new anode material in LIBs was skillfully designed and achieved *via* a facile one-step *in situ* electrochemical self-assembly in which CuCl nanoparticles can act as anode active materials, whereas Cu foil as the anodic current collector. The integrated CuCl/Cu electrode was investigated in terms of XRD, SEM and EDX, galvanostatic charge/discharge, cycle stability, rate performance, CV and AC impedance. Some new insights into inexpensive binder-free CuCl/Cu anodes were gained.

[a]*Faculty of Material Science and Engineering, Kunming University of Science and Technology, Kunming 650093, China. E-mail: hhy@dicp.ac.cn; hongyinghou@kmust.edu.cn; Tel: +86-871-18860731503*

[b]*Faculty of Mechanical and Electronic Engineering, Kunming University of Science and Technology, Kunming 650093, China*

2 Materials and methods

2.1 Binder-free integration of CuCl with the Cu substrate

First, Cu foil (16 mm in diameter, 99.9%) was mechanically polished and rinsed with ethanol and pure water, sequentially. Secondly, binder-free integration of CuCl nanoparticles with Cu foil was achieved by *in situ* one-step anodization of homologous Cu foil in a two-electrode cell containing 0.1 M NaCl and a Pt foil counter electrode. The current density was controlled at 5 mA cm^{-2} for 120 s by an electrochemical workstation (Princeton Parstat 4000, USA). Finally, after rinsing with ethanol, the cleaned electrode was stored in a vacuum drier. The active material can be removed by sonication for a desired time and estimated according to the weight difference before and after sonication. The corresponding loading of CuCl was about 0.20 mg.

2.2 Structure and morphology characterization

The morphology and structure of the integrated CuCl/Cu electrode were probed by SEM (Quanta 200 FEI USA), EDX (APOLLO EDAX, USA) and XRD (TTR III Rigaku Japan) at 40 kV from 20° to 100° (the scan rate: 5° min^{-1}, Cu Kα radiation, $\lambda = 1.5406$ Å). *Ex situ* SEM and XRD experiments were also used to gain insights into the fully charged and discharged electrodes.

2.3 Electrochemical measurements

The electrochemical performances of the integrated CuCl/Cu electrode were investigated by assembling CR2025 coin cells with Li foil as the counter electrode and reference electrode, in which two electrodes were separated by Celgard 2400 polyethylene film, and the electrolyte was 1 M $LiPF_6$ in a mixture of ethylene carbonate and diethyl carbonate (1 : 1 in volume). The coin cell was assembled in an argon-filled glove box (Mikrouna Super 1220/750/900) and measured by galvanostatic charge/discharge from 0.1 V to 3.0 V on a Neware battery testing system (CT-3008W). The charge/discharge rates were 0.2C, 0.5C, 1C and 2C. The electrode area was about 1.1304 cm^2. The corresponding electrochemical performances were evaluated on the same electrochemical workstation in terms of CV curves from 0 to 3 V at 0.5 mV s^{-1} and AC impedance from 100 kHz to 0.01 kHz with a perturbation of 10 mV.

3 Results and discussion

3.1 SEM-EDX

During the anodization, the surface of mirror-like Cu foil was gradually covered by one layer of thin film, and the corresponding SEM images are shown in Fig. 1a and b. As expected, insoluble cubic CuCl nanoparticles did grow and tightly combine with the surface of the Cu substrate, and the mean particle size was about 500 nm. The corresponding chemical component was also obtained, as shown in Fig. 1c. Only the signal peaks corresponding to Cu and Cl elements were visible, indicating the presences of Cu and Cl without other impurities.

3.2 XRD

Fig. 2 shows the XRD spectrum of the integrated electrode, and 6 diffraction peaks were visible. According to literature, 4 diffraction peaks at $2\theta = 28.5°$, 33.1°, 47.4° and 56.3° were assigned to the crystal planes (111), (200), (220) and (311) of CuCl, respectively.[15] Moreover, the other 3 diffraction peaks at $2\theta = 50.4°$, 74.1° and 89.9° corresponded to crystal planes (200), (220) and (311) of the Cu substrate.[16] Clearly, XRD results effectively confirmed the presence of CuCl nanoparticles on the surface of Cu foil together with the SEM-EDX results.

3.3 Mechanism of binder-free integration of CuCl with Cu foil

Based on SEM, EDX and XRD results, the possible reaction mechanism was proposed as follows: the synthesis of CuCl and its binder-free integration with Cu foil were achieved *via* the facile anodization of Cu foil and instantaneous deposition of insoluble CuCl. First, Cu was oxidized into mono-valent Cu^+ after losing an electron under the driving force of the electrical field. Second, Cu^+ *in situ* combined very rapidly with Cl^- on the surface of Cu foil, which was driven by the chemical potential for forming insoluble CuCl on the surface of Cu substrate, as shown in formulas (1) and (2):[17,18]

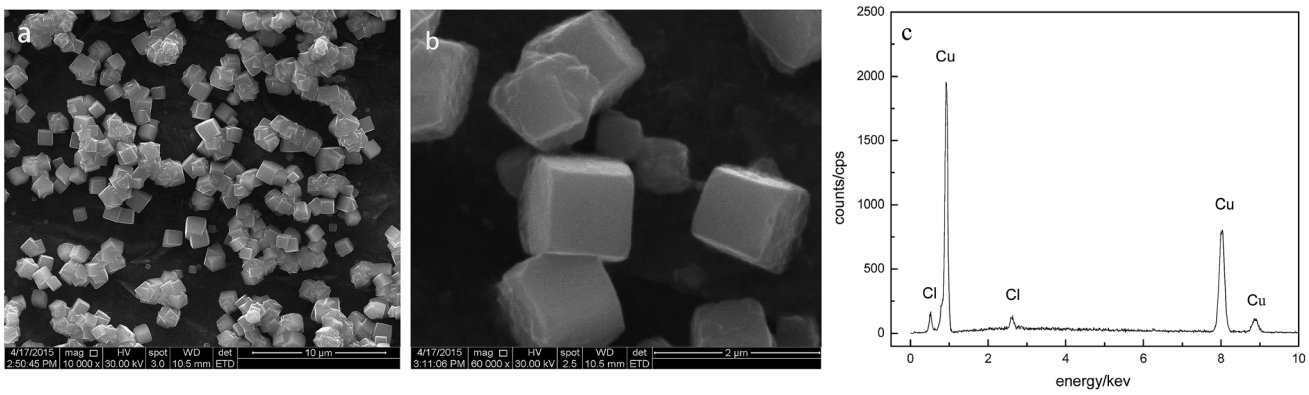

Fig. 1 (a) Low magnification (10 000×) and (b) high magnification (60 000×) top view SEM images of the integrated CuCl/Cu electrode; and (c) EDX spectrum of the integrated CuCl/Cu electrode.

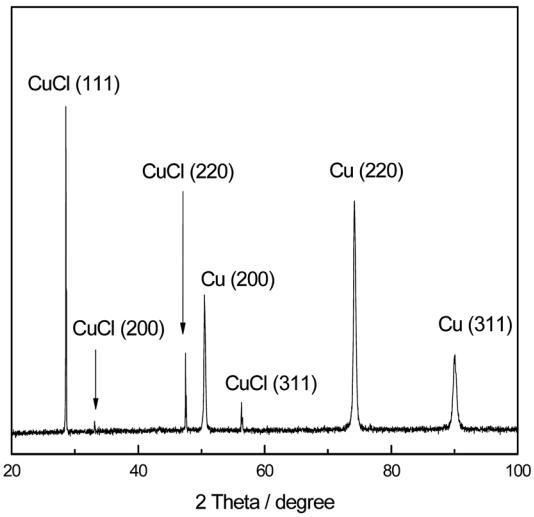

Fig. 2 XRD pattern of the integrated CuCl/Cu electrode.

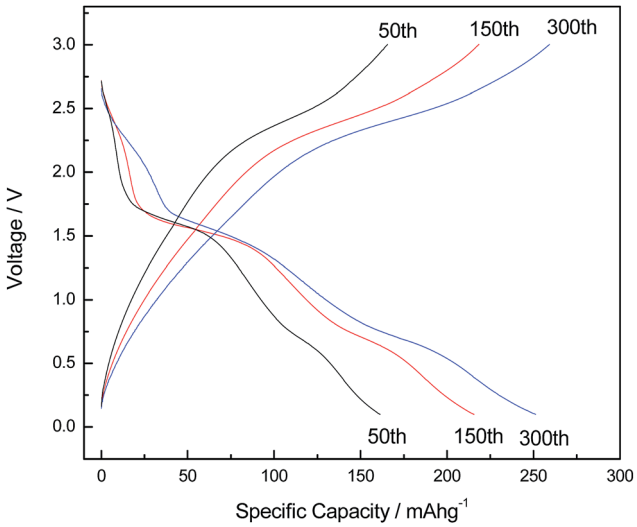

Fig. 3 The 50th, 150th and 300th galvanostatic discharge/discharge curves of the integrated CuCl/Cu electrode at 2C.

$$Cu - e^- \rightarrow Cu^+ \quad (1)$$

$$Cu^+ + Cl^- \rightarrow CuCl\downarrow \quad (2)$$

Finally, CuCl gradually grew up into 500 nm cubic nanoparticles within the reaction time of 120 s and tightly combined with the Cu substrate. Clearly, the integration of CuCl nanoparticles with the Cu foil current collector was automatically achieved without the help of a polymer binder, which was very preferable for fabricating the micro-electrode in a 3D microbattery. Such an integration mechanism is not suitable for synthesis of soluble salts such as $CuCl_2$.

3.4 Charge/discharge performances

As shown in Fig. 3, the 50th, 150th and 300th galvanostatic charge/discharge curves of the integrated CuCl/Cu electrode were measured. It can be observed that the 50th discharge capacity was about 161.3 mA h g^{-1} at 2C. Subsequently, the discharge capacity gradually increased to 215.6 mA h g^{-1} after 150 cycles and to 250.6 mA h g^{-1} after 300 cycles due to a gradual activation process of the electrode. It was proposed that the possible mechanism of the charge/discharge process may include two steps, as illustrated in formulas (3) and (4): first, during the discharge stage, Li^+ diffuses and inserts into the interspaces, or the microstructure CuCl nanoparticles, as a result of the formation of an intermediate composite phase (Li_xCuCl),[19–21] which was also effectively supported by the following CV curves. Second, the conversion reaction of Cu^+ into Cu is accompanied with the formation of a new phase of LiCl. These two processes can also be embodied by the sloping potential ranges of 2.54–1.70 V and 1.66–0.85 V in the discharge curves. The sloping potential range at 0.82–0.10 V corresponded to the formation of the SEI film.[22,23] During the charging stage, all the reactions were inversed.

$$CuCl + xLi^+ + xe^- \leftrightarrow Li_xCuCl \quad (3)$$

$$CuCl + Li^+ + e^- \leftrightarrow Cu + LiCl \quad (4)$$

The increasing tendency of the discharge capacity was also displayed more clearly and intuitively in the cyclic performance in Fig. 4. The corresponding capacity retention was as high as 243.1%, indicating a continuous activation process, which may be jointly caused by the following 3 factors: (i) slow wettability of the integrated CuCl/Cu electrode by the electrolyte;[24] (ii) the large active surface area caused by nano-sized effects;[25,26] (iii) increasing active surface area during the cyclic charge/discharge, which was confirmed by *ex situ* SEM image of the CuCl/Cu electrode after 150 cycles in Fig. 5. For example, it can be observed that the mean particle size of CuCl gradually decreased from 500 nm to 300 nm with the increase of charge/discharge cycles. The smaller size of the particles usually results

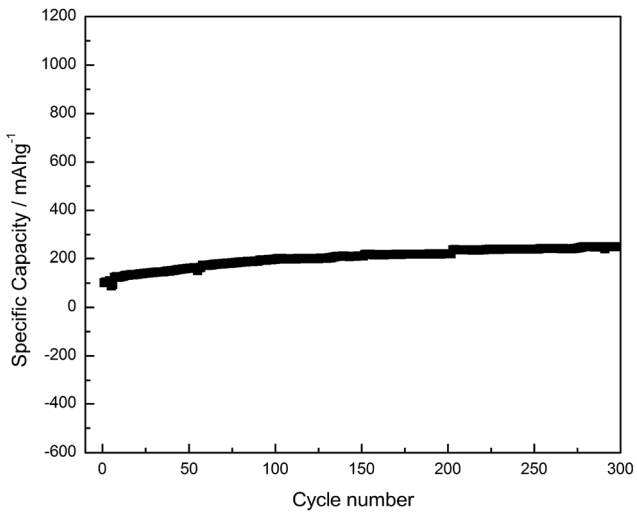

Fig. 4 Cyclic performance of the integrated CuCl/Cu electrode at 2C.

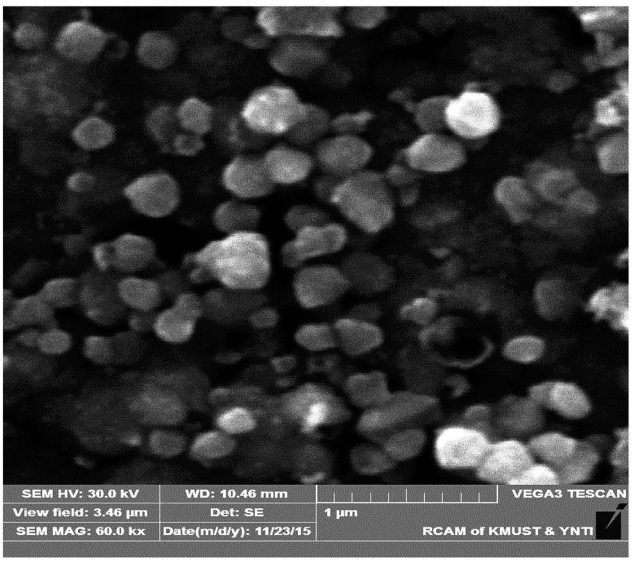

Fig. 5 Ex situ SEM image (60 000×) of the integrated CuCl/Cu electrode after 150 cycles at 2C.

in a larger specific surface area and contact area among CuCl, Cu foil and electrolyte, which can shorten the diffusion path of Li^+ and electrons, and thus enhance the electrochemical performances of the electrode. Interestingly, CuCl nanoparticles still attached firmly onto the surface of the Cu substrate.

3.5 Rate performance

The rate performance of the CuCl/Cu electrode at 0.2C, 0.5C, 1C and 2C, was shown in Fig. 6. With an increase of the rates from 0.2C, 0.5C to 1C, the discharge capacities gradually increased. The corresponding discharge capacities were 267.5 mA h g^{-1}, 297.0 mA h g^{-1} and 306.9 mA h g^{-1}, respectively. Clearly, the discharge capacities at lower rates increased due to the continuous activation process even if the rates slowly increased. The discharge capacity began to decrease when the discharge rate rapidly increased to 2C. Moreover, the discharge rate and the activation of the electrode jointly affected the discharge capacity and the influence of the discharge rate was larger than that of the activation at the higher rate of 2C. Anyway, the binder-free CuCl/Cu electrode exhibited satisfactory rate performance.

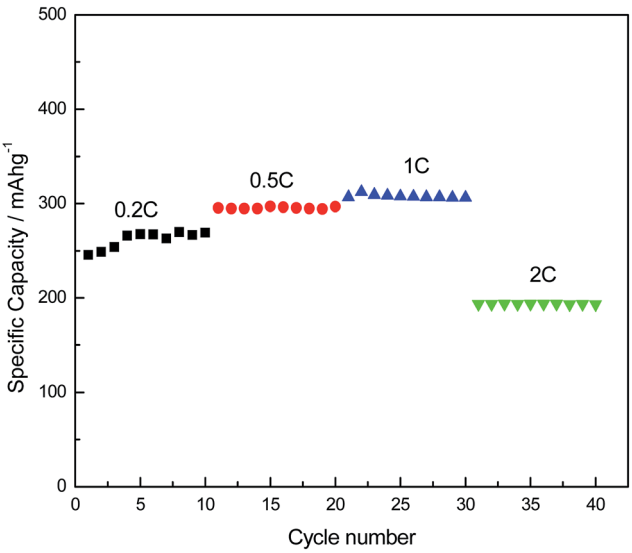

Fig. 6 Rate performance of CuCl/Cu electrode at 0.2C, 0.5C, 1C and 2C.

3.6 CV curve

The charge/discharge mechanism of the CuCl/Cu electrode as mentioned above can be also supported by the CV curve, as shown in Fig. 7. For example, during negative scanning, 3 reduction peaks were detected at 2.41 V, 1.53 V and 0.67 V, corresponding to Li^+ insertion into the interspaces or microstructure of CuCl nanoparticles, the conversion reaction of CuCl nanoparticles with Li^+ into Cu and LiCl, and the formation of SEI film during the discharge.[10,20,22] Moreover, 3 oxidation peaks at 2.45 V, 1.88 V and 1.32 V during positive scanning can be ascribed to the inverse processes, *i.e.*, the conversion reaction of LiCl with Cu to the products of Li^+ and CuCl, Li^+ extraction from the interspaces or microstructure of CuCl nanoparticles and the decomposition of SEI film during the charge, respectively.

3.7 AC impedance analysis

AC impedance spectroscopy is a powerful technique to determine the kinetic parameters of the electrode process. As shown in Fig. 8a, the Nyquist plot of the integrated CuCl/Cu electrode was also obtained *via* AC impedance measurements. Clearly, the Nyquist plot consisted of a compressed semicircle at high frequencies and a straight line at low frequencies, in which the intercept and the diameter of the semicircle at high frequencies on the real axis corresponded to the internal resistance (R_i) and

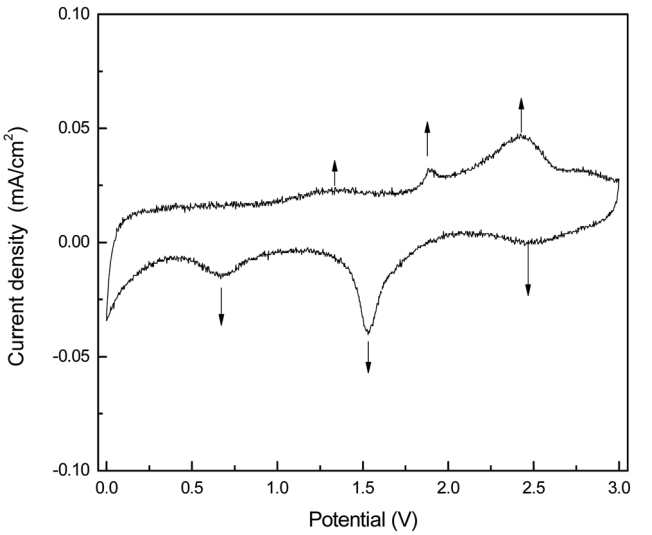

Fig. 7 CV curve of the integrated CuCl/Cu electrode.

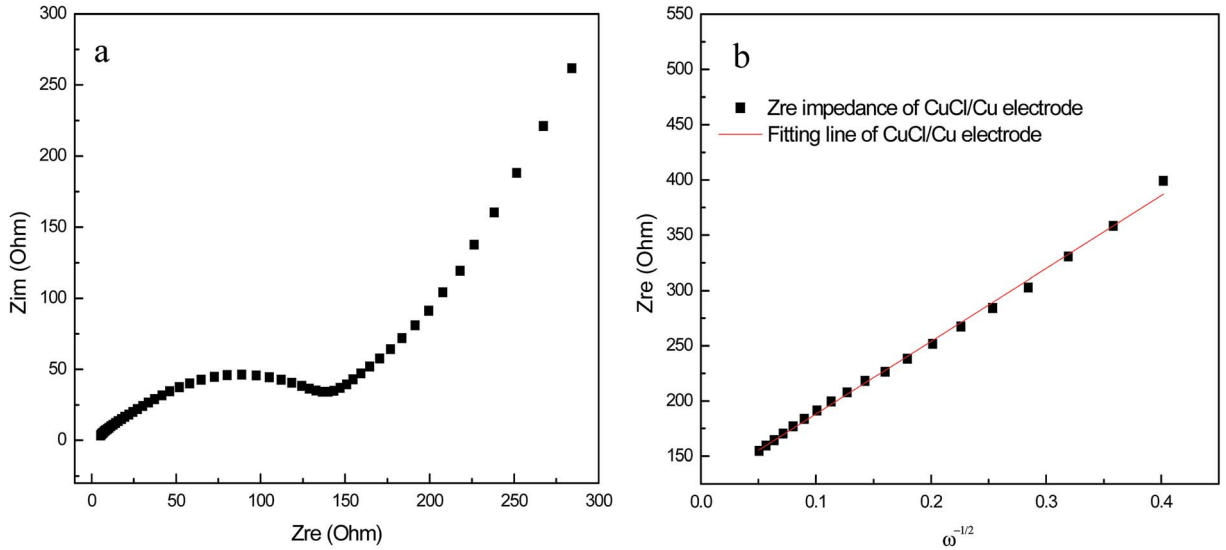

Fig. 8 (a) Nyquist plot of the integrated CuCl/Cu electrode, (b) the line relationship between Z_{re} and $\omega^{-1/2}$ at low frequencies.

the charge transfer resistance (R_{ct}), respectively.[27] In detail, R_i and R_{ct} of the binder-free CuCl/Cu electrode were determined to be 5.4 Ω and 138.3 Ω, respectively, which were reasonable and acceptable. In addition, as indicated in Fig. 8b, the line relationship between Z_{re} at low frequencies and $\omega^{-1/2}$ corresponded to the formula (5):

$$Z_{re} = R_i + R_{ct} + \sigma\omega^{-1/2} \quad (5)$$

where Z_{re} is the real part of the impedance, ω is the angular frequency, and σ is Warburg factor, corresponding to the slope of the fitting line in Fig. 8b. Subsequently, the Li^+ diffusion coefficient (D) of the electrode can be calculated according to eqn (6):[28]

$$D = R^2T^2/(2A^2F^4C^2n^4\sigma^2) \quad (6)$$

where R is the gas constant, T is the absolute temperature, A is the electrode area, F is Faraday's constant, C (7.0×10^{-5} mol cm^{-3}) is the concentration of Li^+ in the electrode,[29] n is the number of reacting electrons, and σ is 659.6 Ω $s^{-1/2}$ according to eqn (5). The Li^+ diffusion coefficient of the integrated electrode was calculated to be 1.8×10^{-11} cm^2 s^{-1}, higher than 4.2×10^{-14} cm^2 s^{-1} of the MnO anode in literature, indicating higher mobility and smaller polarization of Li^+ in the integrated CuCl/Cu electrode.[30]

3.8 Ex situ XRD

To gain insights into the electrochemical conversation reaction mechanism of the CuCl/Cu electrode during the charge/discharge process, *ex situ* XRD was used to further study the structures of fully charging and fully discharging electrodes after 150 cycles, as shown in Fig. 9. It can be found that there were 6 diffraction peaks in the XRD patterns of both electrodes. According to the standard card of JCPDS# 85-1326, 4 diffraction peaks at $2\theta = 43.4°$, 50.4°, 74.1° and 89.9° can be assigned to metallic Cu. As expected, the diffraction peak at $2\theta = 81.6°$ corresponds to the crystal plane (331) of LiCl according to standard card JCPDS# 74-1181, indicating the formation of a new phase of LiCl in the discharge electrode. According to literature, the diffraction peak at $2\theta = 37.6°$ corresponds to the crystal plane (121) of $Cu_2(OH)_3Cl$ (JCPDS# 85-1713) instead of CuCl, possibly due to the fact that CuCl is prone to react with O_2 and H_2O during cleaning of the electrode with pure water prior to testing ex situ XRD, according to formula (7):[31]

$$4CuCl + 4H_2O + O_2 \rightarrow 2Cu_2(OH)_3Cl + 2HCl \quad (7)$$

The presence of CuCl in the charge electrode should be due to the irreversible capacity loss. Clearly, ex situ XRD results

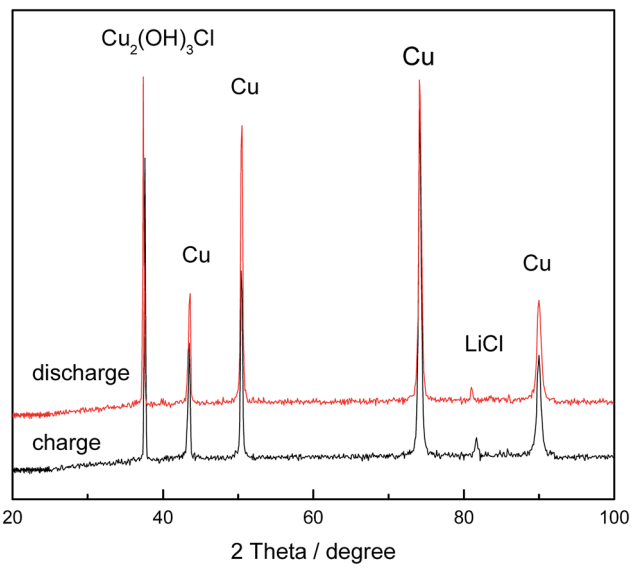

Fig. 9 *Ex situ* XRD patterns of fully charged and fully discharged CuCl/Cu electrodes.

effectively confirmed the proposed conversion reaction mechanism.

4 Conclusions

Binder-free integration of cubic CuCl nanoparticles with a homologous Cu current collector as an LIB anode was designed and achieved *via* a facile one-step electrochemical self-assembly. As expected, insoluble cubic CuCl nanoparticles did grow *in situ* and firmly combined with the surface of Cu foil. Furthermore, the resultant integrated electrode delivered a reversible capacity of 250.6 mA h g^{-1} after 300 cycles at 2C, suggesting the promising feasibility of CuCl as an anode active material in LIBs.

Acknowledgements

This study was financially supported by the National Natural Science Foundation of China (Grant no. 51363011), the 46th Scientific Research Foundation for the Returned Overseas Chinese Scholars, State Education Ministry in China (6488-20130039), the Program of High-level Introduced Talent of Yunnan Province (10978125), Yunnan Project of Training Talent (1418425) and the Project of Key Discipline (14078232 and 14078311).

References

1 H. Guo, X. Li, J. Xie, Z. Wang, W. Peng and Q. Sun, *Energy Convers. Manage.*, 2010, **51**, 247.
2 S. E. Lee, E. Kim and J. Cho, *Electrochem. Solid-State Lett.*, 2007, **10**, A1.
3 N. K. Nitta, F. X. Wu, J. T. Lee and G. Yushin, *Mater. Today*, 2015, **18**, 252.
4 H. Jiang, Y. J. Hu, S. J. Guo, C. Y. Yan, P. S. Lee and C. Z. Li, *ACS Nano*, 2014, 6038.
5 X. F. Chen, Y. Huang, X. Zhang, C. Li, J. J. Chen and K. Wang, *Mater. Lett.*, 2015, **52**, 81.
6 F. W. Zhan, H. Zhang, Y. Qi, J. Z. Wang, N. Du and D. R. Yang, *J. Alloys Compd.*, 2013, **570**, 119.
7 D. Reyter, S. Rousselot, D. Mazouzi, M. Gauthier, P. Moreau, B. Lestriez, D. Guyomard and L. Roue, *J. Power Sources*, 2013, **239**, 308.
8 V. Etacheri, R. Marom, R. Elazari, G. Salitra and D. Aurbach, *Energy Environ. Sci.*, 2011, **4**, 3243.
9 J. W. Zhang, M. M. Zhang and L. J. Zhang, *Electrochim. Acta*, 2013, **105**, 282.
10 Q. B. Zhang, J. X. Wang, J. C. Dong, F. Ding, X. H. Li, B. Zhang, S. H. Yang and K. L. Zhang, *Nano Energy*, 2015, **13**, 77.
11 T. Li, Z. X. Chen, Y. L. Cao, X. P. Ai and H. X. Yang, Transition-metal chlorides as conversion cathode materials for Li-ion batteries, *Electrochim. Acta*, 2012, **68**, 202.
12 J. L. Liu, W. J. Cui, C. X. Wang and Y. Y. Xia, *Electrochem. Commun.*, 2011, **13**, 269.
13 Y. Q. Wang, T. T. Jiang, D. W. Meng, H. Y. Jin and M. H. Yu, *Appl. Surf. Sci.*, 2015, **349**, 636.
14 R. Meng, H. Hou, X. Liu, W. Hu, J. Duan and S. Liu, *Ceram. Int.*, 2015, **41**, 9988.
15 R. C. Yang, X. J. Lu, X. Huang, Z. M. Chen, X. Zhang, M. D. Xu, Q. W. Song and L. T. Zhu, *Appl. Catal., B*, 2015, **170–171**, 225.
16 S. B. Ni, X. H. Lv, T. Li, X. L. Yang and L. L. Zhang, *Electrochim. Acta*, 2013, **109**, 419.
17 H. Y. Huang, D. J. Chien, G. G. Huang and P. Y. Chen, *Electrochim. Acta*, 2012, **65**, 204.
18 S. Emin, F. F. Abdi, M. Fanetti, W. Peng, W. Smith, K. Sivula, B. Dam and M. Valant, *J. Electroanal. Chem.*, 2014, **717–718**, 243.
19 J. W. Mao, X. H. Hou, X. Y. Wang, S. J. Hu and L. Z. Xiang, *Mater. Lett.*, 2015, **161**, 652.
20 J. Cabana, L. Monconduit, D. Larcher and M. R. Palacin, *Adv. Mater.*, 2010, **22**, E170.
21 Y. K. Wang, L. C. Yang, R. Z. Hu, W. Sun, J. W. Liu, L. Z. Ouyang, B. Yuan, H. H. Wang and M. Zhu, *J. Power Sources*, 2015, **288**, 314.
22 J. H. Um, H. Park, Y. H. Cho, M. P. B. Glazer, D. C. Dunand, H. Choe and Y. E. Sung, *RSC Adv.*, 2012, 1.
23 X. Qi, J. Qu, H. B. Zhang, D. Z. Yang, Y. H. Yu, C. Chi and Z. Z. Yu, *J. Mater. Chem. A*, 2015, **3**, 15489.
24 K. Z. Cao, L. F. Jiao, H. Q. Liu, Y. C. Liu, Y. J. Wang, Z. P. Guo and H. T. Yuan, *Adv. Eng. Mater.*, 2015, **5**, 1401421.
25 K. Z. Cao, L. F. Jiao, Y. C. Liu, H. Q. Liu, Y. J. Wang and H. T. Yuan, *Adv. Funct. Mater.*, 2015, **25**, 1082.
26 Y. M. Sun, X. L. Hu, W. Luo, F. F. Xia and Y. H. Huang, *Adv. Funct. Mater.*, 2013, **23**, 2436.
27 G. H. Wu, R. Y. Li, Z. J. Li, J. K. Liu, Z. G. Guo and G. L. Wang, *Electrochim. Acta*, 2015, **172**, 156.
28 C. Wang, D. Higgins, F. F. Wang, D. Y. Li, R. Q. Liu, G. F. Xia, N. Li, Q. Li, H. Xu and G. Wu, *Nano Energy*, 2014, **9**, 334.
29 X. Chen, N. Q. Zhang and K. N. Sun, *J. Mater. Chem.*, 2012, **22**, 13637.
30 G. B. Xu, F. Jiang, Z. A. Ren and L. W. Yang, *Ceram. Int.*, 2015, **41**, 10680.
31 K. F. Chen and D. F. Xue, *J. Phys. Chem. C*, 2013, **117**, 2256.